JACS
JOURNAL OF THE AMERICAN CHEMICAL SOCIETY

Article

pubs.acs.org/JACS

Mapping Structurally Defined Guanine Oxidation Products along DNA Duplexes: Influence of Local Sequence Context and Endogenous Cytosine Methylation

Xun Ming,[†] Brock Matter,[†] Matthew Song,[†] Elizabeth Veliath,[‡] Ryan Shanley,[§] Roger Jones,[‡] and Natalia Tretyakova*,[†]

[†]Department of Medicinal Chemistry and the Masonic Cancer Center and [§]Biostatistics and Bioinformatics Core at the Masonic Cancer Center, University of Minnesota, Minneapolis, Minnesota 55455, United States

[‡]Department of Chemistry and Chemical Biology, Rutgers University, Piscataway, New Jersey 08854, United States

Supporting Information

ABSTRACT: DNA oxidation by reactive oxygen species is nonrandom, potentially leading to accumulation of nucleobase damage and mutations at specific sites within the genome. We now present the first quantitative data for sequence-dependent formation of structurally defined oxidative nucleobase adducts along *p53* gene-derived DNA duplexes using a novel isotope labeling-based approach. Our results reveal that local nucleobase sequence context differentially alters the yields of 2,2,4-triamino-2*H*-oxal-5-one (Z) and 8-oxo-7,8-dihydro-2′-deoxyguanosine (OG) in double stranded DNA. While both lesions are overproduced within endogenously methylated ^{Me}CG dinucleotides and at 5′ Gs in runs of several guanines, the formation of Z (but not OG) is strongly preferred at solvent-exposed guanine nucleobases at duplex ends. Targeted oxidation of ^{Me}CG sequences may be caused by a lowered ionization potential of guanine bases paired with ^{Me}C and the preferential intercalation of riboflavin photosensitizer adjacent to ^{Me}C:G base pairs. Importantly, some of the most frequently oxidized positions coincide with the known *p53* lung cancer mutational "hotspots" at codons 245 (GGC), 248 (CGG), and 158 (CGC) respectively, supporting a possible role of oxidative degradation of DNA in the initiation of lung cancer.

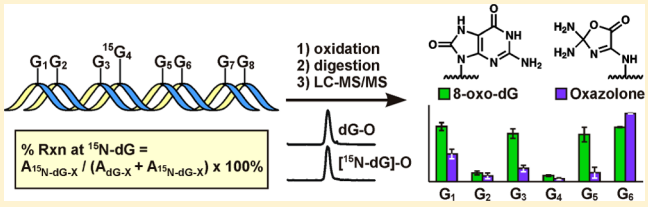

INTRODUCTION

Reactive oxygen species (ROS) and reactive nitrogen species (RNS), e.g., hydrogen peroxide, hydroxyl radical, superoxide, peroxynitrite, and singlet oxygen, are produced physiologically as a result of normal aerobic metabolism, immune response, and inflammation.[1−3] ROS and RNS play a dual role in a living cell: while required for certain cellular processes such as signal transduction and protection against pathogens, they can induce oxidative stress and degradation of cellular biomolecules when formed in excess.[2]

ROS-mediated oxidation of DNA nucleobases has received significant attention in the literature due to its important role in aging, cancer, and neurodegenerative diseases.[4−10] Guanine bases within DNA are preferentially targeted by oxidants due to their relatively low redox potential as compared to the other three nucleobases.[11,12] One-electron oxidation of guanine produces guanine radical cations, which migrate along the π-stack of base pairs within DNA duplexes until being trapped via irreversible reactions with water and/or molecular oxygen to form stable nucleobase adducts (Scheme 1).[13−16]

Guanine oxidation gives rise to more than 10 different DNA lesions, including 8-oxo-7,8-dihydro-2′-deoxyguanosine (OG), spiroiminodihydantoin (Sp), 5-guanidinohydantoin (Gh), and 2,5-diaminoimidazol-4-one (Iz) and its hydrolysis product, 2,2,4-triamino-2*H*-oxal-5-one (Z) (Scheme 1).[17−23] Under aerobic conditions, OG and Z are produced in the highest yield, with typical in vivo concentrations in living cells of 1−10 adducts per 10^7 normal nucleotides.[9,24] OG is prone to further oxidation in the presence of ROS,[14,19−21,25−27] while Z is resistant to further oxidation.[20]

Because electron "hole" pausing at the sites of the lowest ionization potential (IP) increases the probability of stable adduct formation,[12,28−31] DNA oxidation tends to be sequence-dependent.[14,32,33] High resolution gel electrophoresis (PAGE) analysis of DNA strand breaks generated at the sites of nucleobase damage by the action of repair endonucleases or hot piperidine treatment reveals characteristic oxidation patterns.[14,34] Sites containing multiple adjacent guanines, e.g., 5′G < 5′GG < 5′GGG, are preferentially targeted for oxidative adduct formation upon photooxidation, supposedly a result of $\pi-\pi$ stacking and orbital interactions, which lower the IPs of the 5′-guanines in runs of several Gs.[29,32,35,36] Preferential oxidation of two- and three-base runs of Gs have been also reported for other oxidants such as Co^{III}/benzoyl peroxide, carbonate radicals, γ-radiation, and hydroxyl radicals generated by Fenton chemistry (Fe^{2+}−EDTA/H_2O_2).[29,32,37] However, a different sequence specificity was reported for nitrosoperox-

Received: November 14, 2013
Published: February 26, 2014

   dx.doi.org/10.1021/ja411636j | *J. Am. Chem. Soc.* 2014, 136, 4223−4235

Scheme 1. Formation of OG and Z Adducts from Guanine Following One-Electron Oxidation

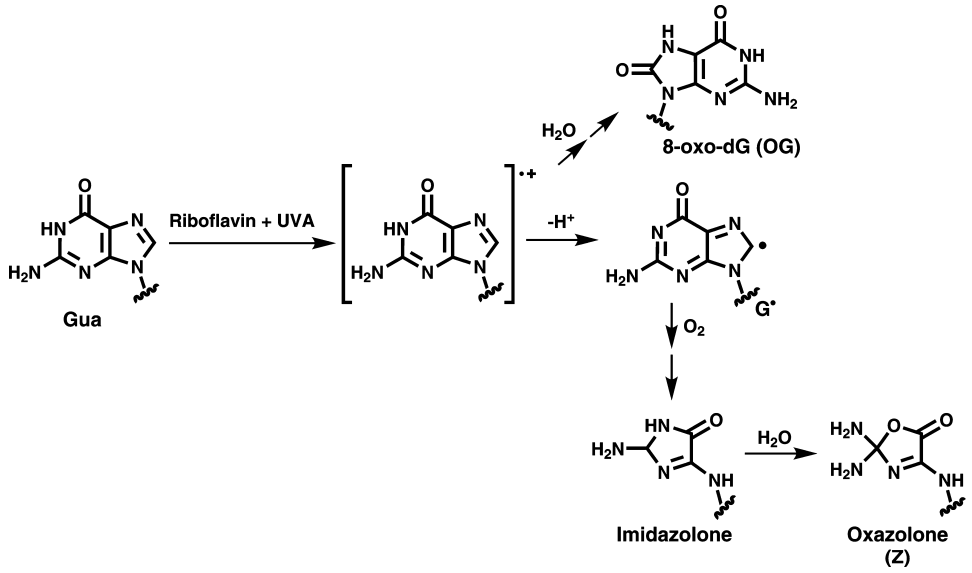

ycarbonate ($ONOO^-$), which reacted preferentially at sites of high IP values, e.g., TGC, AGC, CGC.[32,36]

In addition to nucleotide sequence context, guanine reactivity toward oxidants may be affected by epigenetic DNA modifications, e.g., cytosine methylation to 5-methylcytosine (^{Me}C).[38−40] ^{Me}C bases are formed endogenously by enzymatic methylation of the C5 position of cytosine in CG dinucleotides (CpG sites) and represent about 1% of total bases in the mammalian genome, playing a critical role in gene expression, cell differentiation, host defense, genomic imprinting, and X chromosome inactivation.[41,42] Cytosine methylation has been shown to increase the reactivity of guanine bases in ^{Me}CG dinucleotides toward electrophiles and oxidants. For example, Kawai et al. reported that the rate of electron-transfer quenching of triplet *N,N*-dibutylnaphthaldiimide was increased from 6.8×10^8 M^{-1} s^{-1} for C:G base pair to 8.1×10^8 M^{-1} s^{-1} for ^{Me}C:G base pair, likely due to the transmission of an electronic effect from the ^{Me}C to its partner guanine through hydrogen bonding within the ^{Me}C:G base pair.[38] Preferential oxidation of guanine adjacent to ^{Me}C may contribute to mutational "hot spots" at ^{Me}CG dinucleotides of the *p53* tumor suppressor gene (Figure S1 in the Supporting Information).[43] However, a more recent study by Kanvah et al. did not detect any effect of ^{Me}C on the migration of radical cations along DNA duplexes.[39]

A major limitation of the earlier studies is that oxidative adduct formation was detected indirectly by gel electrophoresis of alkali-generated DNA fragments.[27] This approach provides little structural information about the lesions formed and suffers from a high background due to the direct oxidation of the DNA backbone, which constitutes up to 50% of total damage following treatment with strong oxidants such as γ-radiation.[14,44] A more recent methodology developed by Margolin et al. reduces the background using *Escherichia coli* exonuclease III to remove direct fragments containing direct strand breaks,[32] but does not allow for adduct identification. The resulting oxidative adducts have been classified as "Fpg sensitive lesions" and "piperidine sensitive lesions",[32,36,45] but their actual identities could not be established. This is important because each of the various guanine oxidation products is associated with different biological outcomes in terms of their mutagenic potential and the ability to be removed by repair enzymes.[26,46] For example, secondary oxidation products such as Z, Sp, Gh, and oxaluric acid are significantly more mispairing than OG.[47,48] A QTOF MS method was recently employed to examine the effects of DNA sequence on the susceptibility of OG in DNA toward further oxidation,[49,50] unfortunately, this approach is not suitable for oxidation studies of DNA containing standard DNA bases.

In the present work, stable isotope labeling of DNA−mass spectrometry methodology developed in our laboratory (ILD−MS)[51−54] was employed to accurately quantify OG and Z adducts originating from specific guanine bases within DNA duplexes derived from the *p53* tumor suppressor gene. Our results reveal characteristic patterns of distribution of the two oxidative guanine lesions along DNA duplexes. Adduct yields are influenced by the by the presence of neighboring 5-methylcytosines, flanking sequence, and solvent exposure, with a strong preference for ^{Me}CGG trinucleotides. These results are important because they may provide insight into the origins of mutational hotspots at endogenously methylated CpG sites within the human genome.

MATERIALS AND METHODS

Chemicals. Ammonium acetate, ammonium formate, sodium cacodylic acid, sodium chloride, desferrioxamine, acetonitrile, zinc chloride, Trizma base, methanol, sodium bicarbonate, nuclease P1, alkaline phosphatase, and riboflavin were purchased from Sigma-Aldrich (Milwaukee, WI). Triethylamine and hydrochloric acid were obtained from Fisher Scientific (Hanover Park, IL). $^{15}N_3$,$^{13}C_1$-dG and $^{15}N_3$,$^{13}C_1$-dG phosphoramidites were prepared as described previously (dG: 2′-deoxyguanosine).[55]

Preparation of Nucleoside Adduct Standards. Oxazolone, 8-oxo-dG, and their ^{15}N,^{13}C-labeled analogues were prepared from dG and $^{15}N_3$,$^{13}C_1$-dG as described elsewhere.[24]

DNA Oligodeoxynucleotides. Synthetic oligodeoxynucleotides were prepared by standard phosphoramidite chemistry using an Applied Biosystems ABI 394 DNA synthesizer (Foster City, CA). $^{15}N_3$,$^{13}C_1$-dG was introduced at specified positions by solid phase synthesis using 1,7,NH_2-^{15}N-2-^{13}C-dG phosphoramidite.[55,56] DNA strands containing phenylpyrrolo-C were prepared as described previously.[57,58] All DNA oligomers were purified by HPLC to 99+% purity (Figure S2 in the Supporting Information) and characterized by

dx.doi.org/10.1021/ja411636j | J. Am. Chem. Soc. 2014, 136, 4223−4235

Table 1. Nucleotide Sequence and Mass Spectrometry Characterization (HPLC–ESI-MS/MS) of the Stable Isotope Labeled DNA Oligomers Derived from the *p53* Tumor Suppressor Gene

ID	Sequence	Calculated Molecular Weight	Observed Molecular Weight
[$^{15}N_3$,$^{13}C_1$]-*p53* exon5-G1-Me	CC^{Me}C[$^{15}N_3$,$^{13}C_1$-G]GCACC^{Me}CG^{Me}CGTC^{Me}CG^{Me}CG	5786.0	5785.7
[$^{15}N_3$,$^{13}C_1$]-*p53* exon5-G2-Me	CC^{Me}CG[$^{15}N_3$,$^{13}C_1$-G]CACC^{Me}CG^{Me}CGTC^{Me}CG^{Me}CG	5785.9	5785.7
[$^{15}N_3$,$^{13}C_1$]-*p53* exon5-G3-Me	CC^{Me}CGGCACC^{Me}C[$^{15}N_3$,$^{13}C_1$-G]^{Me}CGTC^{Me}CG^{Me}CG	5785.8	5785.7
[$^{15}N_3$,$^{13}C_1$]-*p53* exon5-G4-Me	CC^{Me}CGGCACC^{Me}CG^{Me}C[$^{15}N_3$,$^{13}C_1$-G]TC^{Me}CG^{Me}CG	5784.9	5785.7
[$^{15}N_3$,$^{13}C_1$]-*p53* exon5-G5-Me	CC^{Me}CGGCACC^{Me}CG^{Me}CGTC^{Me}C[$^{15}N_3$,$^{13}C_1$-G]^{Me}CG	5785.9	5785.7
(-)-*p53* exon5-Me	^{Me}CG^{Me}CGGA^{Me}CG^{Me}CGGGTGC^{Me}CGGG	5981.4	5981.9
[$^{15}N_3$,$^{13}C_1$]-*p53* exon7-G4-Me	ATGGG^{Me}C[$^{15}N_3$,$^{13}C_1$-G]GCATGAAC^{Me}CGGAGGCCCA	7773.7	7774.1
[$^{15}N_3$,$^{13}C_1$]-*p53* exon7-G5-Me	ATGGG^{Me}CG[$^{15}N_3$,$^{13}C_1$-G]CATGAAC^{Me}CGGAGGCCCA	7773.8	7774.1
[$^{15}N_3$,$^{13}C_1$]-*p53* exon7-G6-Me	ATGGG^{Me}CGGCAT[$^{15}N_3$,$^{13}C_1$-G]AAC^{Me}CGGAGGCCCA	7773.7	7774.1
[$^{15}N_3$,$^{13}C_1$]-*p53* exon7-G7-Me	ATGGG^{Me}CGGCATGAAC^{Me}C[$^{15}N_3$,$^{13}C_1$-G]GAGGCCCA	7774.1	7774.1
[$^{15}N_3$,$^{13}C_1$]-*p53* exon7-G8-Me	ATGGG^{Me}CGGCATGAAC^{Me}CG[$^{15}N_3$,$^{13}C_1$-G]AGGCCCA	7774.2	7774.1
[$^{15}N_3$,$^{13}C_1$]-*p53* exon7-G9-Me	ATGGG^{Me}CGGCATGAAC^{Me}CGGA[$^{15}N_3$,$^{13}C_1$-G]GCCCA	7774.0	7774.1
(-)-*p53* exon7-Me	TGGGCCC^{Me}CGGTTCATGC^{Me}CGCCCAT	7614.2	7614.0
[$^{15}N_3$,$^{13}C_1$]-*p53* exon8-G2-Me	GCTTT[$^{15}N_3$,$^{13}C_1$-G]AGGTG^{Me}CGTGTTTGTG	6548.3	6548.9
[$^{15}N_3$,$^{13}C_1$]-*p53* exon8-G3-Me	GCTTTGA[$^{15}N_3$,$^{13}C_1$-G]GTG^{Me}CGTGTTTGTG	6548.3	6548.9
[$^{15}N_3$,$^{13}C_1$]-*p53* exon8-G4-Me	GCTTTGAG[$^{15}N_3$,$^{13}C_1$-G]TG^{Me}CGTGTTTGTG	6548.3	6548.9
[$^{15}N_3$,$^{13}C_1$]-*p53* exon8-G5-Me	GCTTTGAGGT[$^{15}N_3$,$^{13}C_1$-G]^{Me}CGTGTTTGTG	6548.3	6548.9
[$^{15}N_3$,$^{13}C_1$]-*p53* exon8-G6-Me	GCTTTGAGGTG^{Me}C[$^{15}N_3$,$^{13}C_1$-G]TGTTTGTG	6548.3	6548.9
[$^{15}N_3$,$^{13}C_1$]-*p53* exon8-G7-Me	GCTTTGAGGTG^{Me}CGT[$^{15}N_3$,$^{13}C_1$-G]TTTGTG	6548.3	6548.9
(-)-*p53* exon8-Me	CACAAACA^{Me}CGCACCTCAAAGC	6336.2	6336.0
[$^{15}N_3$,$^{13}C_1$]-*p53* exon7-codon245	ATGGGC [$^{15}N_3$,$^{13}C_1$-G]GCATGAAC	4646.1	4645.4
5'-Me-[$^{15}N_3$,$^{13}C_1$]-*p53* exon7-codon245	ATGGG^{Me}C[$^{15}N_3$,$^{13}C_1$-G]GC ATG AAC	4660.1	4659.5
(-)-*p53* exon7-codon245	GTTCATGCCGCCCAT	4504.0	4503.1
(-)-*p53* exon7-codon245-MeC3	GTTCATGC^{Me}CGCCCAT	4518.0	4517.4
[$^{15}N_3$,$^{13}C_1$]-*p53* exon7-codon248	CATGAACC[$^{15}N_3$,$^{13}C_1$-G]GAGGCCCATC	5785.8	5786.8
5'-Me-[$^{15}N_3$,$^{13}C_1$]-*p53* exon7-codon248	CATGAAC^{Me}C[$^{15}N_3$,$^{13}C_1$-G]GAGGCCCATC	5799.8	5800.1
(-)-*p53* exon7-codon248	GATGGGCCTCCGGTTCATG	5835.8	5836.3
(-)-*p53* exon7-codon248-MeC4	GATGGGCCTC^{Me}CGGTTCATG	5849.8	5850.3
[$^{15}N_3$,$^{13}C_1$]-*p53* exon5-codon158	CCCGGCACCCGC[$^{15}N_3$,$^{13}C_1$-G]TCCGCG	5715.7	5714.9
(-)-*p53* exon5-codon158	CGCGGACGCGGGTGCCGGG	5911.9	5910.7
(-)-*p53* exon5-codon158-MeC3	CGCGGA^{Me}CGCGGGTGCCGGG	5925.9	5925.4
(-)-*p53* exon5-codon158-phenylpyrrolo	CGCGGA^{phenylpyrrolo}CGCGGGTGCCGGG	5949.9	5949.6

UV spectroscopy and MALDI mass spectrometry as described previously.[59] The identity and the purity of each DNA strand were further confirmed by HPLC–ESI$^-$-MS (Table 1, Figures S3–S8 in the Supporting Information) (ESI: electrospray ionization). DNA quantification was based on HPLC–UV analysis of dG in enzymatic digests.[60] DNA oligomers were annealed to equimolar amounts of the corresponding complementary strands in the presence of 100 mM NaCl to obtain double-stranded DNA. DNA duplexes were characterized by UV melting and native gel electrophoresis to confirm their purity and stability. All duplexes were characterized by well-defined cooperative melting curves (see example in Figure S10 in the Supporting Information).

Riboflavin-Mediated Photooxidation. A 62.5 μM solution of riboflavin in 20 mM sodium cacodylate (pH 7) and 10 mM NaCl was placed on ice and vigorously bubbled with oxygen gas for 1 min. DNA duplexes (3 nmol, in triplicate) were combined with the oxygenated riboflavin solution to reach the final concentration of 50 μM riboflavin and 40 μM DNA. Samples were transferred to glass vials and suspended in an ice-cold water bath. The solution was irradiated for 20 min with a 60 W tungsten bulb positioned 2 cm from the vial. Following oxidation, samples were promptly transferred to low actinic vials and immediately frozen on dry ice, followed by storage at −80 °C until further processing.

Nitrosoperoxycarbonate Treatment. DNA duplexes (2 nmol in 10 μL of water, in triplicate) were mixed with 3.3 μL of 125 mM sodium bicarbonate/750 mM sodium phosphate buffer, pH 6.9. Following the addition of a 3.3 μL aliquot of 5 mM peroxynitrite solution (Cayman Chemical, Ann Arbor, MI), the solutions were vigorously mixed by vortexing for 30 s, and the reaction mixtures were left at 25 °C for 30 min prior to analysis.

Cobalt/Benzoyl Peroxide Treatment. Isotopically tagged DNA duplexes (2 nmol in 10 μL of water, in triplicate) were mixed with 35 μL of 10 mM sodium cacodylic acid, pH 7. Oxidation was intitiated by adding a 20 μL aliquot of cobalt dichloride solution (50 μM) and 5 μL of benzoyl peroxide solution (1 mM in acetonitrile). Samples were incubated at 37 °C for 5 min and frozen until further processing.

Enzymatic Hydrolysis of DNA. ROS-treated DNA (4.5 nmol) was dissolved in a buffer containing 25 mM ammonium acetate, 2.5 mM zinc chloride, and 5 mM desferrioxamine (DFO) (pH 5.3, total volume 450 μL). DNA was digested to 2′-deoxynucleosides in the presence of nuclease P1 (18 U) and alkaline phosphatase (60 U) for 2 h at 37 °C. The completeness of the enzymatic hydrolysis was confirmed by HPLC–UV of nucleosides (Figure S11 in the Supporting Information).[24] Samples were split into two equal aliquots for separate analyses of oxazolone and OG and immediately fractionated by HPLC or frozen until further analysis.

Off-Line HPC Purification of OG. DNA hydrolysates obtained from 4.5 nmol of DNA were subjected to offline HPLC to enrich for OG. This step was necessary to prevent spontaneous oxidation of dG to OG in DNA hydrolysates, which would interfere with isotope labeling results. A Synergi Hydro-RP HPLC column (4.6 × 250 mm, 4 um, Phenomenex, Torrance, CA) was eluted at a flow rate of 1 mL/min, at 25 °C, with a gradient of 6% methanol in 10 mM ammonium formate, pH 4.2 (solvent A) and acetonitrile (solvent B). Solvent composition was maintained at 0% B from 0 to 32 min, increased to 50% B from 32 to 36 min, kept at 50% B for 4 min, and brought back to 0% B by 43 min, and finally equilibrated at 0% B for 17 min. HPLC fractions containing OG and $^{15}N_3$,$^{13}C_1$-OG (32.6–35.2 min) were collected using an Agilent 1100 fraction collector, immediately frozen on dry ice, and concentrated under vacuum.

Sample Preparation for Analysis of Oxazolone. Enzymatic DNA hydrolysates obtained from 4.5 nmol of DNA were incubated at 25 °C for 18 h to convert imidazolone to oxazolone (Scheme 1).[24] Oxazolone and its $^{15}N_2$,$^{13}C_1$-labeled analogue were isolated by solid

dx.doi.org/10.1021/ja411636j | J. Am. Chem. Soc. 2014, 136, 4223–4235

Scheme 2. Strategy for Isotope Labeling of DNA–Mass Spectrometry (ILD–MS) Based Quantitation of Oxidative Guanine Lesions Originating from Specific Sites within DNA Sequence

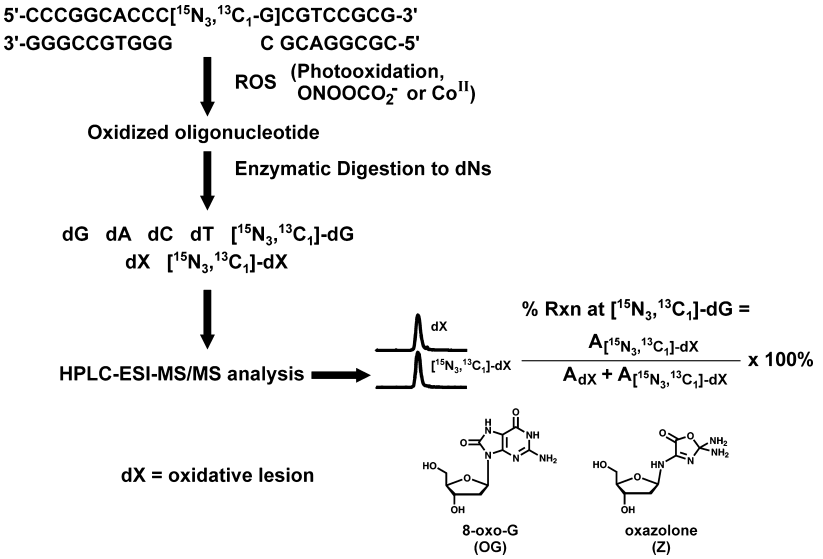

phase extraction using Extract-Clean Carbograph solid phase extraction cartridges (150 mg/4 mL, Grace, Deerfield, IL). The cartridges were equilibrated with methanol and water, followed by sample loading in 1 mL of water. Cartridges were washed with 1 mL of water, and the analyte was eluted with 3 mL of 20% methanol in water. Solid phase extraction (SPE) fractions containing oxazolone and $^{15}N_2$,$^{13}C_1$-oxazolone were dried under reduced pressure and redissolved in 20 μL for analysis by capillary HPLC–ESI-MS/MS.

Capillary HPLC–ESI$^+$-MS/MS of OG and Z. Quantitative analyses of OG and Z in DNA hydrolysates were performed using a Thermo TSQ Quantum Ultra mass spectrometer (Palo Alto, CA) interfaced with a Waters nanoAcquity UPLC system (Milford, MA).

For analyses of oxazolone, a Thermo-Finnigan Hypercarb column (0.5 × 100 mm, 5 μm) was eluted at a flow rate of 12 μL/min with a gradient of 0.05% acetic acid in water (solvent A) and a 3:1 mixture of isopropanol:acetonitrile (solvent B). HPLC solvent composition was gradually changed as follows: 0 min, 1.5% B; 7.1 min, 9.5% B; 7.6 min, 1.5% B; 16 min, 1.5% B. Using this gradient, oxazolone eluted at ~9.4 min. The Thermo TSQ Quantum Ultra triple quadrupole mass spectrometer was operated in the electrospray ionization (ESI) mode, with a spray voltage typically maintained at 2.8 kV and a capillary temperature at 250 °C. Quantitative analyses were performed in the selected reaction monitoring (SRM) mode. The first quadrupole was set to isolate the protonated molecules ($[M + H]^+$) of oxazolone (m/z 247.1) and $^{15}N_2$,$^{13}C_1$-oxazolone (m/z 250.1), and their fragmentation was induced in the second quadrupole serving as a collision cell. Collision-induced dissociation (CID) was performed with Ar as a collision gas (1.0 mTorr) at a collision energy of 14 V. The third quadrupole was set to detect the product ions corresponding to the neutral loss of deoxyribose and CO_2 ($[M + 2H - dR - CO_2]^+$): m/z 87.1 for oxazolone and m/z 90.1 for $^{15}N_2$,$^{13}C_1$-oxazolone. The lower limit of detection for oxazolone was estimated as 5 fmol (S/N = 10). MS parameters were optimized for maximum response during the infusion of standard solutions.

For analysis of OG, an Agilent Extend-C18 column (0.5 × 150 mm, 3.5 um, Agilent, Santa Clara, CA) was eluted isocratically with 13% methanol in 10 mM ammonium formate, pH 4.2, at a flow rate of 11 μL/min. Using this method, OG eluted at ~9.2 min. Typically, ESI was achieved at a spray voltage of 3.2 kV and a capillary temperature of 250 °C. Quantitative analyses were performed in the selected reaction monitoring mode. The first quadrupole was set to isolate the protonated molecules ($[M + H]^+$) of OG (m/z 284.1) and $^{15}N_3$,$^{13}C_1$-OG (m/z 288.1), and their fragmentation was induced in the second quadrupole serving as a collision cell. CID was performed with Ar as a collision gas (1.0 mTorr) at the collision energy of 14 V. The third quadrupole was set to detect the product ions corresponding to the neutral loss of deoxyribose ($[M + 2H - dR]^+$): m/z 168.1 for OG and m/z 172.1 for $^{15}N_3$,$^{13}C_1$-8-oxo-dG. The lower limit of detection for OG was 3 fmol (S/N = 10). MS parameters were optimized for maximum response during the infusion of standard solutions.

Optimization of Oxidation Conditions. Initial experiments have established optimal photooxidation conditions that ensured sequence selectivity for guanine oxidation, but produced sufficient numbers of oxazolone and OG adducts at each guanine to be detected by HPLC–ESI$^+$-MS/MS. Following 20 min photooxidation, ~4% of total DNA strands contained OG and ~2% of strands contained Z (Figure S12 in the Supporting Information). Given the HPLC–ESI$^+$-MS/MS detection limits for OG-dG and Z at 3–5 fmol, we estimated that photooxidation of 3 nmol of DNA should produce sufficient amounts of OG and Z at each guanine to be accurately quantified by our methodology. Similar preliminary experiments have established that DNA treatment with 1 mM nitrosoperoxycarbonate for 30 min and 50 μM Co/benzoyl peroxide treatment for 5 min were optimal for stable isotope labeling experiments (Figure S13 in the Supporting Information).

Data Analysis. The extent of adduct formation at the isotopically tagged guanines (G_x) was calculated from the amounts of ^{15}N,^{13}C-labeled and unlabeled adducts in DNA hydrolysates using the following equation:

$$\%\ \text{oxidation at } G_x = A_{\text{labeled}}/(A_{\text{labeled}} + A_{\text{unlabeled}}) \times 100\%$$

where A_{labeled} and $A_{\text{unlabeled}}$ are the areas under the HPLC–ESI-MS/MS peaks corresponding to the ^{15}N,^{13}C-labeled and unlabeled adducts, respectively.[52] This was repeated for each guanine of interest to determine the distribution of OG and Z along DNA duplexes.

One-way analysis of variance (ANOVA) was used to examine the mean reactivity differences among groups. In cases in which statistically significant differences were revealed by the overall F-test, pairwise group comparisons were conducted using two-sided, two-sample t tests, using the Bonferroni correction for multiple comparisons. Each group's mean percent reactivity was also compared to a theoretical "random" reactivity value, using a two-sided, one-sample t test, with Bonferroni-adjusted p-values. The theoretical value is given by $1/n$, where n is the total number of groups in each set. For all t tests, standard deviation was estimated by the square root of mean squared error (MSE) from ANOVA. All statistical analyses were conducted in SAS (Statistical Analysis Software) version 9.2. The significance level was set at 5%.

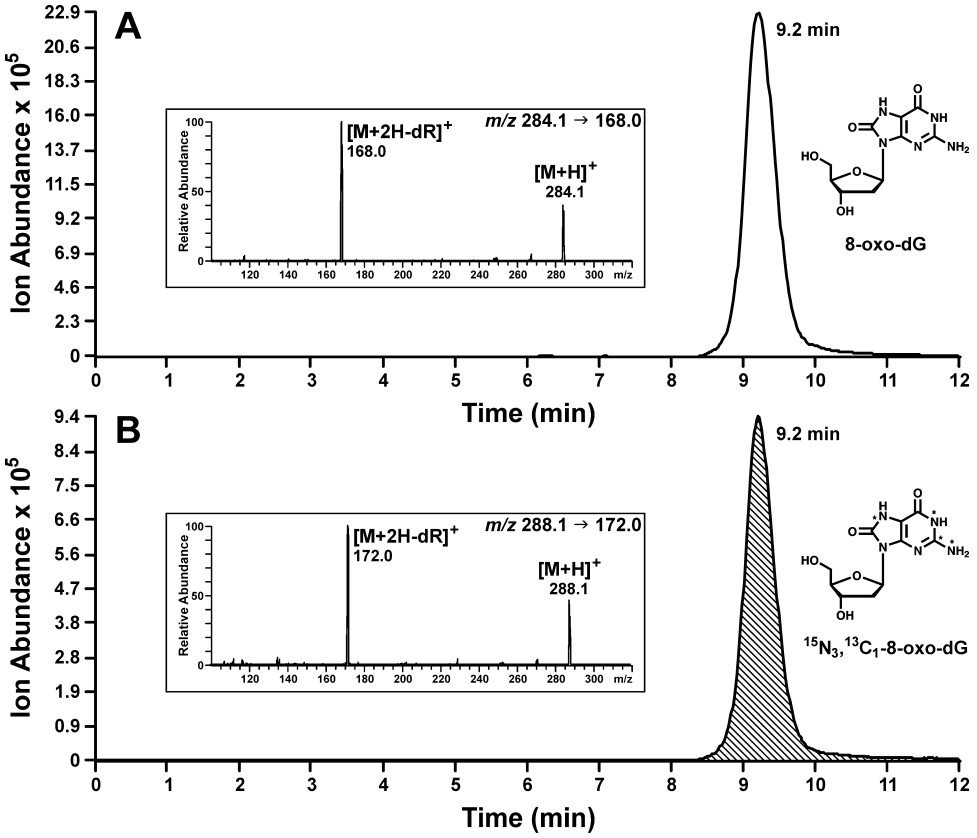

Figure 1. HPLC–ESI$^+$-MS/MS analysis of OG (A) and $^{15}N_3$,$^{13}C_1$-OG (B) in enzymatic hydrolysates of a $^{15}N_3$,$^{13}C_1$-dG containing DNA duplex following photooxidation in the presence of riboflavin. Riboflavin concentration was 62.5 μM, and samples were purged with oxygen for 1 min, followed by irradiation for 20 min at 0 °C.

RESULTS

Influence of Cytosine Methylation on the Formation of OG and Z Adducts on Neighboring Guanine. In the present work, we re-examined the influence of cytosine methylation and local DNA sequence on guanine oxidation using a novel mass spectrometry based approach developed in our laboratory (stable isotope labeling of DNA–mass spectrometry (ILD–MS) (Scheme 2).[52−54,61] In this method, guanine bases within a sequence of interest are replaced with stable isotope-tagged guanine ($^{15}N_3$,$^{13}C_1$-G). Following oxidative treatment, DNA duplexes are enzymatically digested to deoxyribonucleosides, and the relative amounts of OG and Z produced at the $^{15}N_3$,$^{13}C_1$-labeled guanine as compared to other guanine bases are determined by HPLC–ESI$^+$-MS/MS. Since any OG and Z adducts originating from $^{15}N_3$,$^{13}C_1$-G contain the ^{15}N,^{13}C isotope tag, they can be distinguished from lesions formed at other sites by their molecular weight (Scheme 2). We chose three types of oxidants: photoactivated riboflavin (a type I photosensitizer), nitrosoperoxycarbonate (a chemical mediator of inflammation that decomposes to $^{\bullet}NO_2$ and $^{\bullet}CO_3$ radicals), and Co^{II}/benzoyl peroxide, which was used in classical studies of sequence-specific DNA oxidation.[62]

Figures 1 and 2 illustrate HPLC–ESI-MS/MS analysis of site-specific OG and Z adducts originating from a double stranded DNA 19-mer subjected to photooxidation in the presence of riboflavin. Signals specific to OG and $^{15}N_3$,$^{13}C_1$-OG are observed in the corresponding ion channels (m/z 284.1 $[M + H]^+ \rightarrow m/z$ 168.0 $[M + 2H - dR]^+$) and m/z 288.1 $[M + H]^+ \rightarrow m/z$ 172.0, respectively; see Figure 1). Shaded peaks in Figure 1B represent $^{15}N_3$,$^{13}C_1$-OG adducts originating from $^{15}N_3$,$^{13}C_1$-G, while the top panel (Figure 1A) corresponds to unlabeled OG that derive from guanines elsewhere in the sequence. The extent of OG and Z formation at the $^{15}N_3$,$^{13}C_1$-tagged guanine was calculated directly from the HPLC–ESI$^+$-MS/MS areas corresponding to the labeled and unlabeled adducts according to the equation

$$\%\ \text{oxidation at } G_x = A_{\text{labeled}}/(A_{\text{labeled}} + A_{\text{unlabeled}}) \times 100\%$$

where A_{labeled} and $A_{\text{unlabeled}}$ are the areas under the HPLC–ESI-MS/MS peaks corresponding to the ^{15}N,^{13}C-labeled and unlabeled adducts, respectively. Z formation at the guanine of interest was determined analogously using the transitions m/z 247.1 → 87.1 and m/z 250.1 $[M + H]^+ \rightarrow m/z$ 87.2 $[M + 2H - dR - CO_2]^+$, respectively (Figure 2). It should be noted that a +3 rather than +4 mass shift is observed for Z adducts originating from isotopically labeled dG due to a loss of the ^{15}N-nitrogen from the N-2 position of labeled dG during adduct formation (Scheme 1).

Endogenously methylated CG dinucleotides contain two ^{Me}C bases (one per strand). In order to independently examine the effects of base paired ^{Me}C and 5′ neighboring ^{Me}C on guanine reactivity toward oxidants, methylated cytosine was placed in either one or both strands of synthetic DNA duplexes (Table 2). These sequences were derived from the *p53* tumor suppressor gene and represent endogenously methylated CG dinucleotides frequently mutated in lung cancer and surrounding sequence. UV melting experiments confirmed that DNA was completely in the duplex form (example in Figure S10 in the Supporting Information). The extent of adduct formation at

dx.doi.org/10.1021/ja411636j | J. Am. Chem. Soc. 2014, 136, 4223−4235

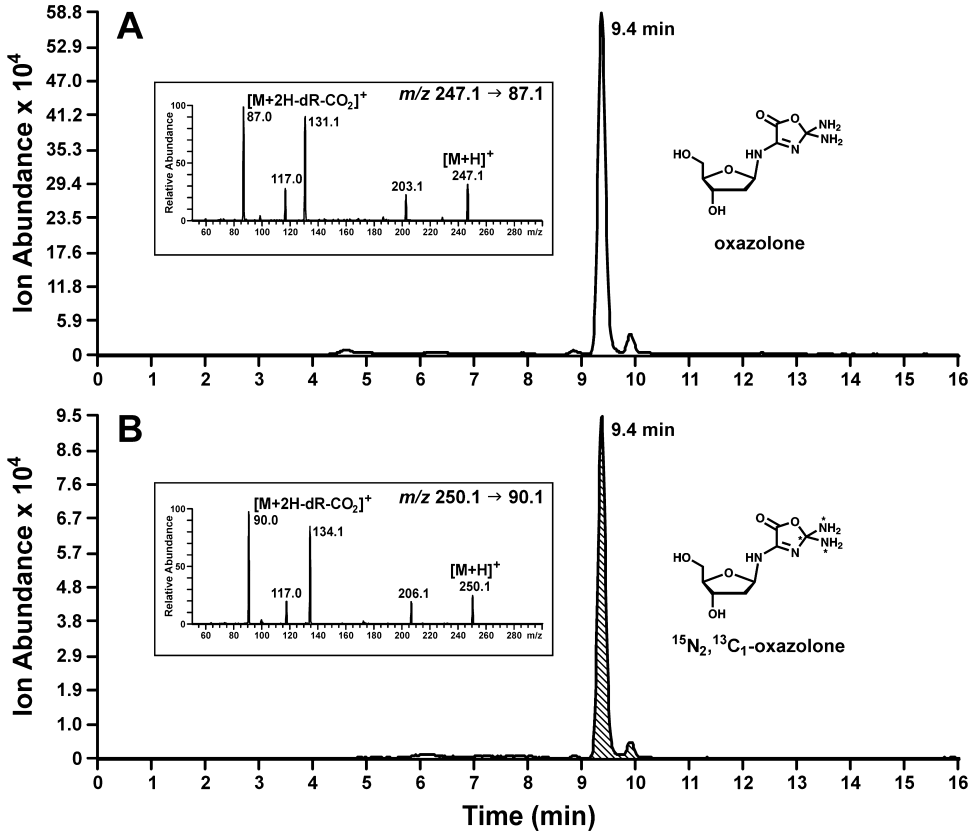

Figure 2. HPLC–ESI$^+$-MS/MS analysis of Z (A) and $^{15}N_2$,$^{13}C_1$–Z (B) in enzymatic hydrolysates of a $^{15}N_3$,$^{13}C_1$–dG containing DNA duplex subjected to photooxidation in the presence of riboflavin. See Figure 1 for photooxidation conditions.

Table 2. DNA Duplexes Used To Elucidate the Influence of Cytosine Methylation within CG Dinucleotides on Guanine Reactivity toward Reactive Oxygen Species

Methylated site	DNA duplex
p53 codon 245	5′-ATGGGC[$^{15}N_3$,$^{13}C_1$-G]GCATGAAC-3′ 3′-TACCC G C CGTACAAG-5′
	5′-ATGGG^{Me}C[$^{15}N_3$,$^{13}C_1$-G]GCATGAAC-3′ 3′-TACCC G C CGTACAAG-5′
	5′-ATGGGC [$^{15}N_3$,$^{13}C_1$-G]GCATGAAC-3′ 3′-TACCC G ^{Me}C CGTACAAG-5′
	5′-ATGGG^{Me}C[$^{15}N_3$,$^{13}C_1$-G]GCATGAAC-3′ 3′-TACCC G ^{Me}C CGTACAAG-5′
p53 codon 248	5′-CATGAACC[$^{15}N_3$,$^{13}C_1$-G]GAGGCCCATC-3′ 3′-GTACTTGG C CTCCGGGTAG-5′
	5′-CATGAAC ^{Me}C[$^{15}N_3$,$^{13}C_1$-G]GAGGCCCATC-3′ 3′-GTACTTG G C CTCCGGGTAG-5′
	5′-CATGAACC[$^{15}N_3$,$^{13}C_1$-G]GAGGCCCATC-3′ 3′-GTACTTGG ^{Me}C CTCCGGGTAG-5′
	5′-CATGAAC ^{Me}C[$^{15}N_3$,$^{13}C_1$-G]GAGGCCCATC-3′ 3′-GTACTTG G ^{Me}C CTCCGGGTAG-5′
p53 codon 157	5′-CCCGGCACCCGC[$^{15}N_3$,$^{13}C_1$-G]TCCGCG-3′ 3′-GGGCCGTGGGCG C AGGCGC-5′
	5′-CCCGGCACCCGC[$^{15}N_3$,$^{13}C_1$-G]TCCGCG-3′ 3′-GGGCCGTGGGCG ^{Me}C AGGCGC-5′
	5′-CCCGGCACCCGC[$^{15}N_3$,$^{13}C_1$-G]TCCGCG-3′ 3′-GGGCCGTGGGCG ^{phenylpyrrolo}C AGGCGC-5′

the $^{15}N_3$-labeled guanine was normalized to the adduct yields at the same guanine in the absence of ^{Me}C, which was set to 100%.

For DNA sequences derived from *p53* codons 245 and 248, introduction of methyl group on cytosine immediately 5′ of the target G (^{Me}CG) or at the base paired cytosine (^{Me}C:G) facilitated riboflavin-mediated photooxidation, with the highest adduct yields observed in fully methylated dinucleotides (both 5′ and base paired ^{Me}C, see Figures 3A and 3B). Specifically, OG adduct formation at the $^{15}N_3$,$^{13}C_1$-labeled G in codon 245 nearly doubled when ^{Me}C was placed immediately preceding the target guanine (192%, $p < 0.0001$), increased by 70% in the presence of methyl group at the base paired cytosine (177.5%, $p < 0.0001$), and more than doubled in fully methylated dinucleotide (212%, $p < 0.0001$) (Figure 3A, white bars). Similar results were observed for Z (Figure 3A, black bars). A much more pronounced effect of ^{Me}C was observed for ^{Me}C located within the context of *p53* codon 248. In this case, the introduction of ^{Me}C opposite target G led to a 9-fold increase of Z adduct yields, while the 5′-neighboring ^{Me}C caused a 4-fold increase in adduct formation (Figure 3B). In contrast, OG yields were only increased by 20–30% relative to the corresponding unmethylated *p53* codon 248.

These results suggest that while cytosine methylation facilitates guanine oxidation in both CpG dinucleotides examined, the extent of methylation-mediated increase and the relative quantities of the oxidation products are dependent upon surrounding DNA sequence. We hypothesize that the fate of riboflavin-induced guanine radical cation intermediate (Scheme 1) is influenced by the local DNA structure, leading to different amounts of individual oxidation products in different sequence contexts. It is possible that neighboring bases alter solvent accessibility of the guanine radical cation intermediate ($G^{\cdot+}$, Scheme 1) and/or facilitate its deprotonation, leading to different fractions of guanine radical cations being ultimately converted to 8-oxo-dG vs oxazolone.

dx.doi.org/10.1021/ja411636j | J. Am. Chem. Soc. 2014, 136, 4223–4235

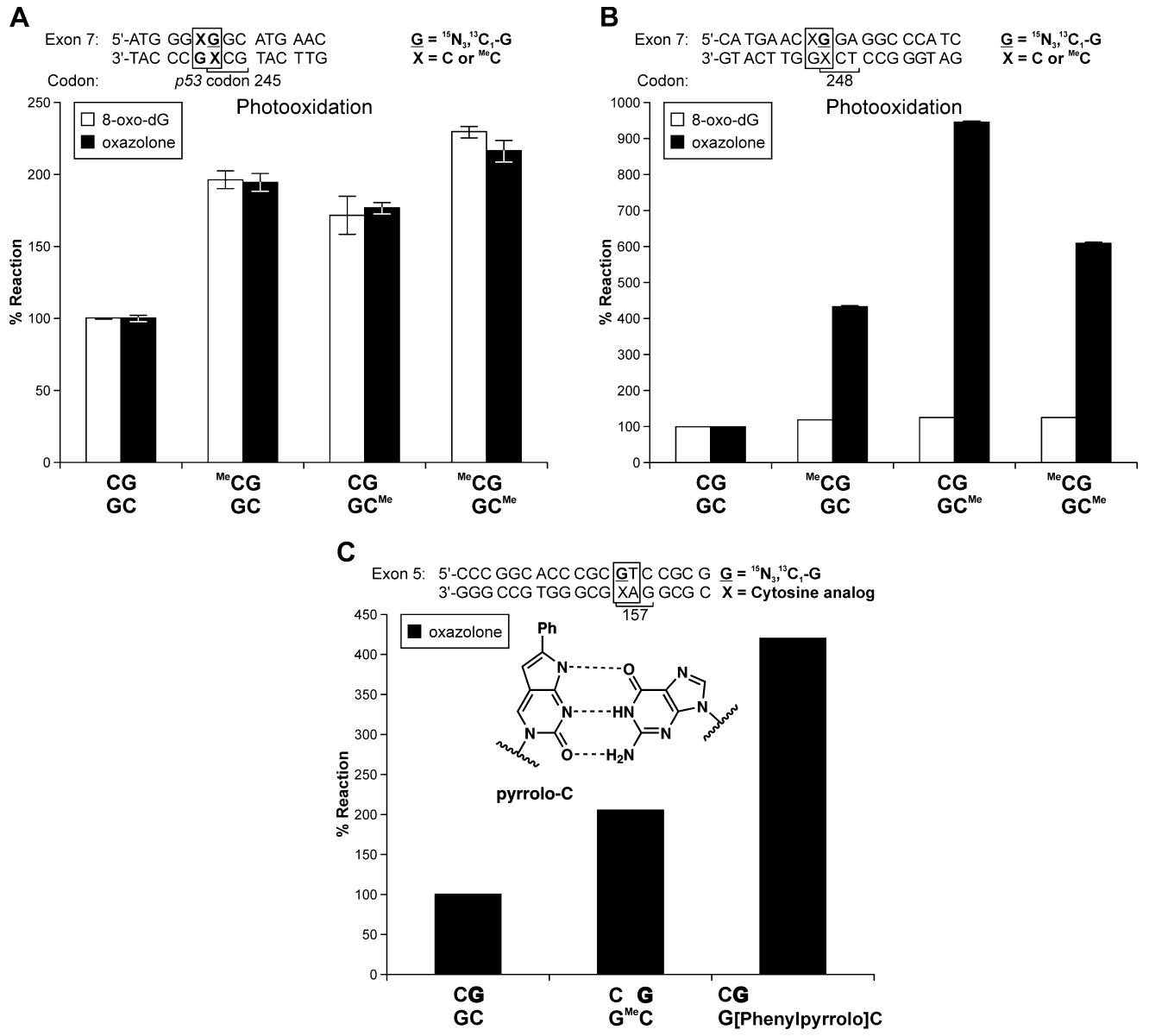

Figure 3. Influence of cytosine methylation within CG dinucleotides on the formation of OG (white bars) and Z adducts (black bars) upon riboflavin-mediated photooxidation: *p53* codon 245 (A) and *p53* codon 248 (B). Panel C shows the relative yields of Z adducts at guanine paired with ^{Me}C and phenylpyrrolo-C. Isotopically tagged G was placed in a DNA duplex opposite dC, 5-methylcytosine, or phenylpyrrolo-C, followed by photooxidation in the presence of riboflavin. Z adduct formation at the labeled G was quantified by HPLC–ESI-MS/MS as shown in Scheme 2. Error bars correspond to standard deviation of three independent measurements.

In theory, ^{Me}C may accelerate the rate of photooxidation of neighboring guanine bases in the presence of riboflavin-mediated oxidants by affecting the local geometry and the electronics of C:G pairs or by facilitating the intercalation of riboflavin photosensitizer adjacent to ^{Me}C:G base pairs. To evaluate potential role of riboflavin intercalation to the increased oxidative lesion yields at the at ^{Me}CG sites, ^{Me}C was replaced with phenylpyrroloC, an unnatural cytosine analogue known to facilitate $\pi-\pi$ stacking interactions with flat aromatic molecules such as riboflavin.[57,58] We found that Z yields at phenylpyrroloC-G base pairs were even greater than in the presence of ^{Me}C (Figure 3C). This is consistent with the idea that riboflavin intercalation at endogenously methylated CG dinucleotides contributes to the increased OG and Z adduct formation at ^{Me}CG sites within the *p53* gene.

To determine whether ^{Me}C-mediated increase in guanine oxidation was specific for riboflavin-mediated reactions, ILD–MS experiments were repeated with two additional oxidants, chemical mediator of inflammation nitrosoperoxycarbonate and Co^{II}/benzoyl peroxide. Unlike riboflavin, nitrosoperoxycarbonate and cobalt are unable to participate in stacking interactions with ^{Me}C, therefore any reactivity changes observed upon the introduction of methylated cytosine are likely attributed to the electronic effects. We found that the presence of neighboring ^{Me}C had a relatively small effect on Co^{II}/benzoyl peroxide-mediated guanine oxidation (black bars in Figure 4), but significantly increased the formation of Z adducts upon treatment with nitrosoperoxycarbonate (striped bars in Figure 4).

The observed differences between the effects of cytosine methylation on nitrosoperoxycarbonate-mediated guanine

dx.doi.org/10.1021/ja411636j | J. Am. Chem. Soc. 2014, 136, 4223–4235

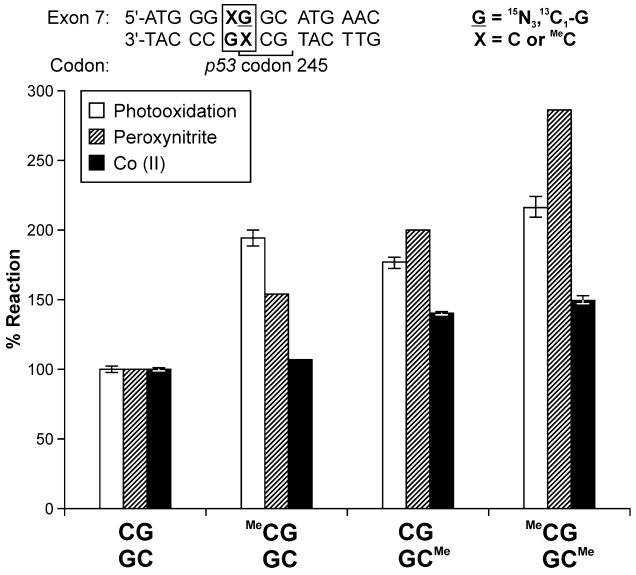

Figure 4. Influence of cytosine methylation within *p53* codon 245 on oxidative adduct yields (Z) on isotopically labeled guanine (G) following oxidation of DNA duplexes in the presence of photosensitized riboflavin (white bars), nitrosoperoxycarbonate (striped bars), and Co^{II}/benzoyl peroxide (black bars). Error bars correspond to standard deviation of three independent measurements.

oxidation as compared to riboflavin-induced photooxidation (Figure 4) could be explained by different nature of the reactive oxygen species participating in reaction with the target guanine. Both $CO_3^{\bullet}$ and triplet riboflavin are strong oxidants, with reduction potentials of 1.59 and 1.7 V versus NHE, respectively.[37] However, photoactivated riboflavin-mediated oxidation of DNA involves photosensitizer intercalation into the DNA duplex, followed by a direct electron transfer from dG to riboflavin, producing guanine radical cation (Scheme 1).[63] In contrast, $ONOOCO_2^-$-mediated oxidation of guanine is mediated by $CO_3^{\bullet}$ radicals and does not require intercalation.[37] The photosensitizer intercalation step is likely to be differentially affected by 5-methylC adjacent to the target G versus the base paired 5-methylC, leading to different oxidative adduct yields in these two duplexes. Future computational and experimental studies are needed to test this hypothesis. Taken together, our results suggest that endogenous cytosine methylation targets neighboring guanine bases for the preferential oxidation by a combination of two mechanisms: electronic effects that lower the IP of guanine bases in ^{Me}CG dinucleotides[38] and stacking interactions that facilitate the intercalation of riboflavin photosensitizer adjacent to ^{Me}C:G base pairs.

Distribution of OG and Z in Riboflavin-Mediated Photooxidation in *p53* Gene-Derived DNA Duplexes. In humans, ^{Me}C is found predominantly at CG dinucleotides, with about 80% of all CG sites endogenously methylated in somatic cells.[64] While many of the ^{Me}CG sequences in the human genome are found at "CpG islands" of regulatory sequences that control the levels of gene expression, some of them are located within coding sequences of genes.[43] Specifically, all CG dinucleotides of the *p53* tumor suppressor gene are endogenously methylated.[65] The same sites, e.g., *p53* codons 158, 245, 248, and 273, are the major "hotspots" for mutations in smoking-induced lung cancer (Figure S1 in the Supporting Information), leading to the hypothesis that tobacco carcinogens may preferentially modify endogenously methylated ^{Me}CG dinucleotides.[66] We and others have previously reported that N^2-BPDE-dG adducts of carcinogenic polycyclic aromatic hydrocarbons such as benzo[*a*]pyrene are preferentially formed at ^{Me}CG dinucleotides of the *p53* tumor suppressor gene, specifically codons 157, 158, 245, 248, and 273.[43,52,58,59,67,68]

To examine whether cytosine methylation preferentially targets endogenously methylated CG dinucleotides of the *p53* gene for oxidative degradation, a series of isotopically tagged oligodeoxynucleotides were synthesized representing specific regions of the *p53* gene derived from exons 5, 7, and 8 (Table 1). These were selected because they contain codons 157, 158, 245, 248, and 273 frequently mutated in lung cancer (Figure S1 in the Supporting Information). ^{Me}C was inserted in both strands at all endogenously methylated CG sites as observed physiologically (Table 1). Isotopically tagged strands were annealed to the complementary strands, and duplex formation was confirmed by UV melting experiments. Following riboflavin-mediated photooxidation and DNA hydrolysis, the extent of OG and Z formation at each location of interest along this duplex was calculated based on isotope ratio HPLC–ESI^+-MS/MS as shown in Scheme 2 and Figures 1 and 2.

Exon 7 Derived Sequence. Our initial isotope labeling experiments were conducted with DNA duplexes derived from *p53* codons 243–250 (5′-ATG$_1$ G$_2$G$_3$ ^{Me}C **G$_4$G$_5$**C AT**G$_6$** AAC ^{Me}C**G$_7$G$_8$** A**G$_9$**G$_{10}$ CCC A-3′) where ^{Me}C = endogenous 5-methylcytosine) (Table 1). $^{15}N_3$,$^{13}C_1$-dG was introduced at one of the highlighted positions (**G$_4$**, **G$_5$**, **G$_6$**, **G$_7$**, **G$_8$**, or **G$_9$**, Table 1), and ^{Me}C was inserted at the two endogenously methylated sites (^{Me}C **G$_4$** and ^{Me}C**G$_7$**).

Since the *p53* exon-7-derived duplex contains a total of 17 guanines, a sequence-independent (random) oxidation would lead to 5.88% of oxidative lesion occurring at each individual guanine (100%/17 = 5.88%). However, OG adduct numbers are significantly above the average value at two distinct sites, **G$_4$** (codon 245) and **G$_7$** (codon 248), which give rise to 18.7 and 14.2% of total OG adducts, respectively (white bars in Figure 5A). Similar results are observed for Z, with 15.9% of adducts originating from **G$_4$** and 18.1% coming from **G$_7$** (black bars in Figure 5A). Importantly, both sites of the highest reactivity (**G$_4$** and **G$_7$**) have an identical sequence context (^{Me}CGG), with the target G flanked by another guanine at the 3′ side and a methylated cytosine on the 5′ side (Figure 5A). The same two sites correspond to prominent lung cancer mutational hotspots at *p53* codons 245 and 248, respectively (Figure S1 in the Supporting Information).[43,68,69] In contrast, the remaining guanine bases exhibited below average reactivity (Figure 5A) and are infrequently mutated in lung cancer.[43,68,69] Studies with the corresponding single stranded oligonucleotides revealed essentially random reactivity (Figure S14 in the Supporting Information), confirming that the presence of intact double stranded DNA is required for the observed sequence selectivity. Overall, our results for fully methylated *p53* exon 7 duplex (Figure 5A) are consistent with the data for short duplexes containing single methylated CpG sites (Figure 3A,B). However, the magnitude of the effect observed upon cytosine methylation differs between the two experiments, probably due to the presence of other neighboring methylated CpG sites in the fully methylated duplex.

Exon 5 Derived Sequence. In order to further investigate the effects of DNA sequence on the formation of oxidative guanine lesions, isotope labeling studies were extended to *p53* gene exon 5. This region of the *p53* gene contains several additional

dx.doi.org/10.1021/ja411636j | *J. Am. Chem. Soc.* 2014, 136, 4223–4235

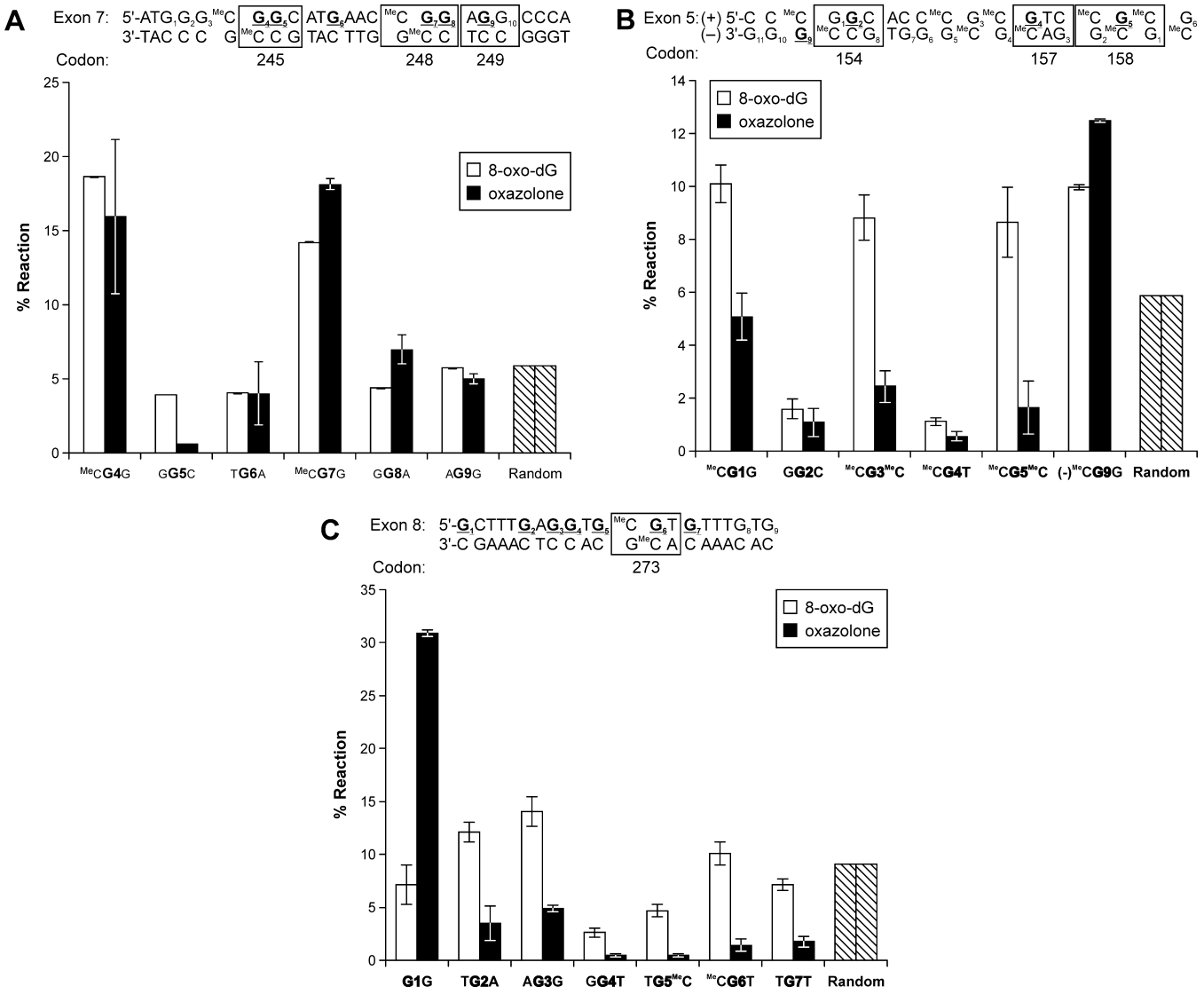

Figure 5. Distribution of OG (white bars) and Z lesions (black bars) along DNA duplexes derived from *p53* exon 7 (A), *p53* exon 5 (B), and *p53* exon 8 (C) following oxidation in the presence of photosensitized riboflavin as determined by stable isotope labeling. Error bars correspond to standard deviation of 3–5 independent measurements.

mutational "hotspots" characteristic for smoking-induced lung cancer, e.g., codons 154 (G**G**C), 157 (**G**TC), and 158 (C**G**C), all containing endogenous 5-methylcytosine (^{Me}CG).[70] In our experiments, the highlighted guanines ($\mathbf{G_1}$, $\mathbf{G_2}$, $\mathbf{G_3}$, $\mathbf{G_4}$, or $\mathbf{G_5}$) were sequentially replaced with $^{15}N_3$,$^{13}C_1$-dG (Table 1), and ^{Me}C was incorporated at all physiologically methylated 5′-CG sites: 5′-CC^{Me}C $\mathbf{G_1G_2}$C ACC ^{Me}C$\mathbf{G_3}$ ^{Me}C $\mathbf{G_4}$TC ^{Me}C$\mathbf{G_5}$ ^{Me}C G$_6$ [(+) strand] (Table 1).[65] Following riboflavin-mediated photooxidation and DNA hydrolysis of the isotopically labeled duplexes, the amounts of OG and Z originating from each location were calculated from HPLC–ESI$^+$-MS/MS isotope ratios as described above (Scheme 2).

Unlike our results for exon 7 derived duplexes, which showed similar distribution patterns of both oxidative adducts (Figure 5A), the patterns of Z and OG formation along the duplexes derived from exon 5 were quite different from each other (Figure 5B). While OG was preferentially formed at $\mathbf{G_1}$, $\mathbf{G_3}$, and $\mathbf{G_5}$, Z yields were below 5% for all guanines tested within (+) strand of DNA (less than the predicted random reactivity value of 5.88%, see Figure 5B). In general, the formation of OG followed the following order: $\mathbf{G_1}$ ($^{Me}C\mathbf{G_1}G_2$) > $\mathbf{G_3}$ ($^{Me}C\mathbf{G_3}^{Me}C$) ≈ $\mathbf{G_5}$ ($^{Me}C\mathbf{G_5}^{Me}C$) ≫ $\mathbf{G_2}$ ($G_1\mathbf{G_2}C$) ≈ $\mathbf{G_4}$ ($^{Me}C\mathbf{G_4}T$) (Figure 5B, white bars). The sites of the highest OG formation included a guanine flanked by 5′-G and a 3′-^{Me}C (^{Me}C$\mathbf{G_1}$G) and two sites flanked by two 5-methylcytosines (^{Me}C**G**^{Me}C, $\mathbf{G_3}$ and $\mathbf{G_5}$).

To identify the sites of preferential Z formation in this duplex, we conducted an additional isotope labeling experiment for guanine 9 of the (−) strand (Figure 5B). We found that (−) G$_9$ (G**G**^{Me}C sequence context) was highly susceptible to photooxidation, giving rise to over 13% of total Z adducts (Figure 5B). The same sequence was identified as the main target for photooxidation within *p53* exon 7 (Figure 5A). Taken together, our results for *p53* exon 7 indicate that the two oxidative lesions (OG and Z) have distinct distribution patterns within this region of the genome, but share one target sequence (G**G**^{Me}C). Furthermore, one of the sites favored for OG production ($\mathbf{G_5}$) coincides with a known *p53* lung cancer mutational hotspot at codon 158, while the other two frequently adducted sites ($\mathbf{G_1}$ and **G3**) do not.

dx.doi.org/10.1021/ja411636j | J. Am. Chem. Soc. 2014, 136, 4223–4235

Exon 8 Derived Sequence. The third *p53*-derived sequence examined (5′-$\mathbf{G_1}$CT TT$\mathbf{G_2}$ A$\mathbf{G_3}$$\mathbf{G_4}$ T$\mathbf{G_5}$^{Me}C $\mathbf{G_6}$T$\mathbf{G_7}$ TTT $\mathbf{G_8}$T$\mathbf{G_9}$) corresponds to a frequently mutated region of *p53* exon 8 and contains an important smoking-associated lung cancer mutational "hotspot" at codon 273 (CGT → CTT) (Figure S1 in the Supporting Information).[43,71] Initial isotope labeling studies conducted with *p53* exon 8-derived duplexes have revealed that OG formation was the highest at $\mathbf{G_3}$ (A$\mathbf{G_3}$$\mathbf{G_4}$) and $\mathbf{G_2}$ (T$\mathbf{G_2}$A) (Figure 5C). In contrast, Z yields were well below the theoretical random reactivity value (7.7%) at all Gs examined, with the exception of the terminal guanine ($\mathbf{G_1}$), which gave rise to over 30% of total Z adducts (Figure 5C, black bars). These results suggest that Z, but not OG adducts, are overproduced at solvent exposed sites such as the ends of DNA duplexes. Interestingly, Lee et al. have previously reported that the formation of photooxidation-induced alkali-labile lesions (such as Z) was facilitated at guanines adjacent to an abasic site as a result of increased solvent exposure.[72] This may facilitate the formation of tandem DNA lesions, which are more difficult to repair and may add to the mutagenic and toxic effects of oxidative stress.

DISCUSSION

Oxidative DNA damage is a key contributor to the pathogenesis of smoking-induced lung cancer.[73,74] Tobacco smoke contains high concentrations of nitric oxide (NO), which can be oxidized to the nitrating and oxidizing agent, nitrogen dioxide.[75−77] Furthermore, phenolic and polyphenolic species present in cigarette tar and formed during carcinogen metabolism can undergo redox cycling yielding superoxide anion radicals, $O_2^{-\bullet}$.[73] Superoxide combines with NO at a diffusion controlled rate to yield peroxynitrite, $ONOO^-$, which conjugates with carbon dioxide to form a strong oxidant, nitrosoperoxycarbonate $ONOOCO_2^-$.[77] $O_2^{-\bullet}$ is also subject to spontaneous or enzymatic dismutation to hydrogen peroxide (H_2O_2), which can undergo the Fenton reaction with Fe^{2+} to produce highly reactive hydroxyl radicals ($HO^\bullet$).[78]

Smoking is associated with increased levels of DNA oxidation.[8,74,79] Cigarette smokers excrete elevated amounts of the oxidative DNA lesion, OG-7,8-dihydro-2′-deoxyguanosine (OG) in urine, which is reversed upon smoking cessation.[79] OG levels are also increased in leukocyte DNA of smokers as compared with nonsmoking controls.[73] The increased cellular load of oxidative DNA lesions in the tissues of smokers is likely to play a role in lung tumor induction. For example, knockout mice deficient at repairing oxidative lesions are predisposed to the development of lung adenocarcinoma.[80] It has been shown that smokers who exhibit low levels of hOgg1, a repair protein responsible for the removal of OG and other oxidative lesions, are at an increased risk of lung cancer.[8] If unrepaired, these oxidized bases are strongly mispairing, inducing large numbers of G → T and G → C transversions.[47]

Of the multiple genes mutated in lung cancer, the *p53* tumor suppressor gene is among the most important. P53 protein is involved in multiple important cellular processes, including cell cycling, gene transcription, chromosomal segregation, DNA repair, and apoptosis.[81,82] The *p53* gene is frequently mutated in smoking-induced lung cancer,[66] with the majority of genetic changes being G → T transversions at *p53* exons 5, 7, and 8 (Figure S1 in the Supporting Information). Prominent *p53* mutational "hotspots" include codons 154 (*GGC* → *GTC*), 157 (*GTC* → *TTC*), 158 (*CGC* → *CTC*), 245 (*GGC* → *TGC*), 248 (*CGG* → *CTG*), 249 (*AGG* → *ATG*), and 273 (*CGT* → *CTT*) (Figure S1 in the Supporting Information).[83,84] Most of these sites correspond to guanines within endogenously methylated dinucleotides (^{Me}CG, where ^{Me}C = 5-methycytosine). Because *p53* exons 5−8 encode the DNA binding domain of the *p53* protein, mutations within these regions inactivate the protein, contributing to cancer initiation and progression.[85] However, the chemical origins of the *p53* gene mutations observed in lung cancer have not been established, although several studies have implicated DNA damage induced by polycyclic aromatic hydrocarbons and aldehydes present in tobacco smoke.[69,83]

In the present work, an isotope labeling of DNA−mass spectrometry based approach developed in our laboratory[51,52] was used to quantify the formation of OG and Z lesions at specific guanine bases within DNA duplexes derived from the *p53* tumor suppressor gene. These lesions are among the major guanine oxidation products produced by a variety of oxidative treatments, including riboflavin-mediated photooxidation, exposure to superoxide radicals, and nitrosoperoxycarbonate treatment.[1,18] While OG is readily oxidized to secondary products,[19,21,86] Z is resistant to further oxidation.[24] Mapping oxidative DNA lesions along critical regions of the *p53* tumor suppressor gene and probing their association with *p53* mutational "hotspots" may provide an insight into the origin of mutational hotspots observed in smoking-induced lung cancer. The main advantage of the isotope labeling methodology as compared to gel electrophoresis-based methods is that it provides robust structural information for oxidized nucleobases, in addition to accurate sequence distribution data.

In order to map the distribution of OG and Z adducts, synthetic DNA duplexes derived from a frequently mutated region of the *p53* tumor suppressor gene were prepared in which guanine bases of interest were sequentially replaced with $^{13}C_1$,$^{15}N_3$-guanine (Tables 1 and 2). Following photooxidation in the presence of riboflavin or treatment with other reactive oxygen species, DNA was enzymatically digested to 2′-deoxynucleosides, and the formation of OG and Z adducts at each site was accurately quantified by isotope ratio HPLC−ESI$^+$-MS/MS (Scheme 2, Figures 1 and 2).

We found that OG and Z formation within duplexes derived from the *p53* tumor suppressor gene was nonrandom (Figure 5). In general, OG yields followed the following order: ^{Me}C**G**G > ^{Me}C**G**T ≈ ^{Me}C **G**^{Me}C ≈ A**G**G > T**G***T* > T**G**A ≈ G**G**C ≈ C**G**T ≈ T**G**C ≈ G**G**A ≈ G**G**T. While Z and OG adducts exhibited similar sequence preferences in the central regions of DNA duplexes, the formation of Z lesions was strongly favored at solvent exposed regions at the ends of DNA duplexes (e.g., G1 in Figure 5C). This can be explained by the effects of sequence context and base pairing on the fate of their common intermediate, the guanine radical cation produced upon one-electron oxidation of G ($G^{\bullet+}$, Scheme 1). Deprotonation of $G^{\bullet+}$ ($pK_a \sim 3.9$) produces neutral guanine radicals ($G^\bullet$), which react with oxygen and generate Z as the main final product (Scheme 1).[1] In a stable DNA duplex, base pairing of G with C in the opposite strand prevents such deprotonation, causing the radical cation intermediate to react with water and generate OG (Scheme 1).[87] As a result, Z, but not OG adducts, are specifically overproduced at the ends of DNA duplexes where Watson−Crick base pairing of target Gs to the complementary strand may be disrupted,[72] e.g., $\mathbf{G_1}$ in *p53* exon 8-derived duplex (Figure 5C) and $\mathbf{G_9}$ in exon 5-derived sequence (Figure 5B). These results suggest that the yield of highly mutagenic Z adducts may be increased at the regions of genome where base pairing is transiently or permanently compromised (e.g., base

dx.doi.org/10.1021/ja411636j | *J. Am. Chem. Soc.* 2014, 136, 4223−4235

mispairs or actively transcribed regions).[37] In contrast, OG and Z formation in single stranded DNA exhibits little sequence specificity, consistent with a requirement for charge transport along DNA duplex (Figure S14 in the Supporting Information).

In central regions of DNA with intact duplex structure, OG and Z adduct yields are determined by two main factors: nucleobase sequence and methylation status of neighboring cytosines. Both lesions are preferentially formed at endogenously methylated CG dinucleotides and in runs of several Gs, with the highest reactivity observed at central Gs of ^{Me}C**G**G sequences (Figure 5). The increased reactivity of 5′-Gs of guanine runs toward one-electron oxidants is well documented.[14,29,88] It has been proposed that electron holes are preferentially trapped at guanine residues located in the 5′-position to another guanine (e.g., 5′-GG or 5′-GGG).[14,35] Ab initio calculations suggest that these are the most electron-rich sites in the B-form of DNA and therefore may act as thermodynamical "sinks" for oxidative damage following long-range charge transport from other sites in the helix (G-G stacking rule).[15,89]

Perhaps the most important result of this study is the enhanced oxidation of guanines within endogenously methylated ^{Me}CG dinucleotides (Figures 3−5). These methylated sequences are preferentially oxidized in the presence of photosensitized riboflavin, nitrosoperoxycarbonate, and Co^{II}/benzoyl peroxide (Figure 4). All CG dinucleotides within the coding region of the *p53* gene contain 5-methylcytosine,[65] and many of these sites are known mutational "hot spots" for smoking induced lung cancer (Figure S1 in the Supporting Information).[68] Furthermore, targeted oxidation of ^{Me}CG sequence can induce epigenetic changes, as OG has been reported to inhibit human DNA methyltransferases.[90]

Previous experimental and computational studies have revealed that the nucleophilicity of guanine bases within ^{Me}C:G base pairs is enhanced as a result of the inductive electronic effects of the C-5 methyl group transmitted to the N^2-amino group of G through ^{Me}C:G hydrogen bonds.[91] Consistent with this explanation, the presence of electron withdrawing fluoro group on the C-5 of cytosine reduces the reactivity of G:C base pairs toward electrophiles.[91] Kawai et al. employed triplet-quenching experiments to show that the one-electron oxidation rate of guanine was accelerated upon hydrogen bonding with 5-methylcytosine.[38] An opposite effect was observed when C-5 methyl group was replaced with an electron withdrawing bromo substituent.[38] These studies suggest that the transmitted electronic effect of the methyl group may be an important factor responsible for the accelerated oxidation of guanine bases within endogenously methylated ^{Me}CG dinucleotides.

In addition to its electronic effects, the presence of C5-methyl group increases the molecular polarizability of cytosine, decreases the major groove charge density, stabilizes DNA helix, and enhances base stacking.[92,93] We have previously reported that C-5 cytosine alkylation facilitates the formation of intercalative complexes of diolepoxide metabolites of polycyclic aromatic hydrocarbons with DNA, facilitating the nucleophilic attack by the N^2 position of guanine and increasing the guanine adduct yields.[58] Our present results suggest that the presence of ^{Me}C can similarly stabilize intercalative complexes of riboflavin photosensitizer with DNA via increased $\pi-\pi$ stacking interactions, leading to increased yields of oxidative guanine adducts at methylated CG dinucleotides. Indeed, even greater Z yields were observed upon phootoxidation of phenylpyrroloC:G base pairs (Figure 3C). PhenylpyrroloC is a highly aromatic analogue of ^{Me}C previously shown to participate in intercalative complex formation with flat polycondensed aromatic molecules.[58] This finding suggests that riboflavin intercalation adjacent to ^{Me}C:G base pairs enhances initial electron transfer and facilitates subsequent oxidation steps.

Our results differ from an earlier report that employed PAGE methodology to examine the influence of cytosine methylation on long-distance radical cation transport following electron hole injection into duplexes containing anthraquinone photosensitizer covalently linked to the 5′-terminus.[39] One possible explanation is that the earlier study[39] was limited to two specific DNA sequences (TCGCGT and AGGT) and did not include CGG trinucleotides as found in the *p53* gene (Figure 5). Furthermore, our results may differ because the approach employed in this work (ILD−MS)[51] quantifies specific DNA adducts (OG and Z) rather than determining total numbers of all alkali sensitive lesions by gel electrophoresis. Finally, our photooxidation experiments intentionally employed riboflavin in solution rather than covalently linked photosensitizer, allowing for precovalent interactions to contribute to the observed sequence specificity for photooxidation. Typical riboflavin (vitamin B2) concentrations in human plasma are ∼300 nM, where it plays an important role in oxidative folding and secretion of proteins including apolipoprotein B-10.[94] It is also present in the cell nucleus and has been reported to act as a photosensitizer, damaging DNA in vivo following UVA irradiation.[95] However, it should be noted that cytosine methylation also increased oxidative adduct yields on neighboring guanines following treatment with other ROS such as nitrosoperoxycarbonate and Co^{II}/benzoyl peroxide (Figure 4). These results are consistent with the electronic effect of the methyl group transmitted through hydrogen bonding within the ^{Me}C:G base pair.[38,91] Interestingly, ^{Me}C itself has been recently identified as an oxidation "hotspot" when mispaired with A or T.[40]

In summary, our isotope labeling results indicate that both OG and Z are preferentially generated at endogenously methylated ^{Me}CG dinucleotides and at the 5′ Gs in runs of several guanines. The central guanines in ^{Me}C**G**G sequences are highly susceptible to oxidation. In addition, Z but not OG adducts are overproduced at solvent exposed regions of DNA such as the ends of DNA duplexes. These results are important because they provide the first sequence distribution data for structurally defined oxidative guanine adducts, contributing to our understanding of DNA oxidation chemistry, and may help uncover the origins of mutational "hotspots" found at endogenously methylated CG dinucleotides within the human genome. Future studies are needed to establish whether the same sequence specificity for oxidation is maintained in chromosomes of human cells. However, it should be noted that ^{Me}CG sites may also be targeted by other electrophiles due to the increased reactivity of guanine bases adjacent to ^{Me}C.[58,69] Furthermore, the *p53* mutational spectra found in lung tumors are likely to be affected by sequence-dependent repair,[96] mispairing efficiency, and biological selection of mutants for growth.

■ ASSOCIATED CONTENT

Ⓢ Supporting Information

Distribution of mutations in human lung cancer mapped along exons 5−8 of the *p53* gene, representative HPLC−UV trace demonstrating DNA purity, HPLC−ESI-MS data for synthetic

DNA oligomers, representative UV melting curves, HPLC traces of enzymatic DNA digests, formation of Z and OG adducts in synthetic DNA duplex following photooxidation and treatment with nitrosoperoxycarbonate, and distribution of OG lesions along single-stranded DNA derived from *p53* exon 7 as determined by stable isotope labeling. This material is available free of charge via the Internet at http://pubs.acs.org.

AUTHOR INFORMATION

Corresponding Author

trety001@umn.edu

Notes

The authors declare no competing financial interest.

ACKNOWLEDGMENTS

We thank Robert H. E. Hudson (University of Western Ontario) for providing phenylpyrrolo-dC phosphoramidite for these studies, Delshanee Kotandeniya (University of Minnesota Cancer Center) for preparing and purifying some of the synthetic oligonucleotides, and Robert Carlson (University of Minnesota Cancer Center) for finalizing the figures for this manuscript. This study was supported by a grant from the National Cancer Institute (CA-095039).

REFERENCES

(1) Cadet, J.; Douki, T.; Ravanat, J. L. *Free Radical Biol. Med.* **2010**, *49*, 9−21.
(2) Valko, M.; Rhodes, C. J.; Moncol, J.; Izakovic, M.; Mazur, M. *Chem. Biol. Interact.* **2006**, *160*, 1−40.
(3) Evans, M. D.; Dizdaroglu, M.; Cooke, M. S. *Mutat. Res.* **2004**, *567*, 1−61.
(4) Bennett, M. R. *Circ. Res.* **2001**, *88*, 648−650.
(5) Canella, K. A.; Diwan, B. A.; Gorelick, P. L.; Donovan, P. J.; Sipowicz, M. A.; Kasprzak, K. S.; Weghorst, C. M.; Snyderwine, E. G.; Davis, C. D.; Keefer, L. K.; Kyrtopoulos, S. A.; Hecht, S. S.; Wang, M.; Anderson, L. M.; Rice, J. M. *In Vivo* **1996**, *10*, 285−292.
(6) Malins, D. C.; Holmes, E. H.; Polissar, N. L.; Gunselman, S. J. *Cancer* **1993**, *71*, 3036−3043.
(7) Greenberg, M. M. *Biochem. Soc. Trans.* **2004**, *32*, 46−50.
(8) Paz-Elizur, T.; Krupsky, M.; Blumenstein, S.; Elinger, D.; Schechtman, E.; Livneh, Z. *J. Natl. Cancer Inst.* **2003**, *95*, 1312−1319.
(9) Helbock, H. J.; Beckman, K. B.; Shigenaga, M. K.; Walter, P. B.; Woodall, A. A.; Yeo, H. C.; Ames, B. N. *Proc. Natl. Acad. Sci. U.S.A.* **1998**, *95*, 288−293.
(10) Malins, D. C. *Environ. Health Perspect.* **1996**, *104*, 1140.
(11) Steenken, S.; Jovanovic, S. V. *J. Am. Chem. Soc.* **1997**, *119*, 617−618.
(12) Prat, F.; Houk, K. N.; Foote, C. S. *J. Am. Chem. Soc.* **1998**, *120*, 845−846.
(13) Elias, B.; Shao, F.; Barton, J. K. *J. Am. Chem. Soc.* **2008**, *130*, 1152−1153.
(14) Burrows, C. J.; Muller, J. G. *Chem. Rev.* **1998**, *98*, 1109−1152.
(15) Nunez, M. E.; Rajski, S. R.; Barton, J. K. *Methods Enzymol.* **2000**, *319*, 165−188.
(16) Yun, B. H.; Lee, Y. A.; Kim, S. K.; Kuzmin, V.; Kolbanovskiy, A.; Dedon, P. C.; Geacintov, N. E.; Shafirovich, V. *J. Am. Chem. Soc.* **2007**, *129*, 9321−9332.
(17) Cadet, J.; Treoule, R. *Photochem. Photobiol.* **1978**, *28*, 661−667.
(18) Douki, T.; Cadet, J. *Free Radical Res.* **1996**, *24*, 369−380.
(19) Luo, W.; Muller, J. G.; Rachlin, E. M.; Burrows, C. J. *Org. Lett.* **2000**, *2*, 613−616.
(20) Niles, J. C.; Wishnok, J. S.; Tannenbaum, S. R. *Org. Lett.* **2001**, *3*, 963−966.
(21) Luo, W.; Muller, J. G.; Rachlin, E. M.; Burrows, C. J. *Chem. Res. Toxicol.* **2001**, *14*, 927−938.
(22) Ravanat, J. L.; Cadet, J. *Chem. Res. Toxicol.* **1995**, *8*, 379−388.
(23) Cadet, J.; Berger, M.; Buchko, G. W.; Joshi, P. C.; Raoul, S.; Ravanat, J. L. *J. Am. Chem. Soc.* **1994**, *116*, 7403−7404.
(24) Matter, B.; Malejka-Giganti, D.; Csallany, A. S.; Tretyakova, N. *Nucleic Acids Res.* **2006**, *34*, 5449−5460.
(25) Tretyakova, N. Y.; Niles, J. C.; Burney, S.; Wishnok, J. S.; Tannenbaum, S. R. *Chem. Res. Toxicol.* **1999**, *12*, 459−466.
(26) Tretyakova, N. Y.; Wishnok, J. S.; Tannenbaum, S. R. *Chem. Res. Toxicol.* **2000**, *13*, 658−664.
(27) Tretyakova, N. Y.; Burney, S.; Pamir, B.; Wishnok, J. S.; Dedon, P. C.; Wogan, G. N.; Tannenbaum, S. R. *Mutat. Res.* **2000**, *447*, 287−303.
(28) Kino, K.; Saito, I.; Sugiyama, H. *J. Am. Chem. Soc.* **1998**, *120*, 7373−7374.
(29) Saito, I.; Nakamura, T.; Nakatani, K.; Yoshioka, Y.; Yamaguchi, K.; Sugiyama, H. *J. Am. Chem. Soc.* **1998**, *120*, 12686−12687.
(30) Hirakawa, K.; Yoshida, M.; Oikawa, S.; Kawanishi, S. *Photochem. Photobiol.* **2003**, *77*, 349−355.
(31) Hirakawa, K.; Suzuki, H.; Oikawa, S.; Kawanishi, S. *Arch. Biochem. Biophys.* **2003**, *410*, 261−268.
(32) Margolin, Y.; Shafirovich, V.; Geacintov, N. E.; DeMott, M. S.; Dedon, P. C. *J. Biol. Chem.* **2008**, *283*, 35569−35578.
(33) Kanvah, S.; Joseph, J.; Schuster, G. B.; Barnett, R. N.; Cleveland, C. L.; Landman, U. *Acc. Chem. Res.* **2010**, *43*, 280−287.
(34) Ndlebe, T.; Schuster, G. B. *Org. Biomol. Chem.* **2006**, *4*, 4015−4021.
(35) Saito, I.; Takayama, M.; Nakamura, T.; Sugiyama, H.; Komeda, Y.; Iwasaki, M. *Nucleic Acids Symp. Ser.* **1995**, 191−192.
(36) Margolin, Y.; Cloutier, J. F.; Shafirovich, V.; Geacintov, N. E.; Dedon, P. C. *Nat. Chem. Biol.* **2006**, *2*, 365−366.
(37) Lee, Y. A.; Yun, B. H.; Kim, S. K.; Margolin, Y.; Dedon, P. C.; Geacintov, N. E.; Shafirovich, V. *Chemistry* **2007**, *13*, 4571−4581.
(38) Kawai, K.; Wata, Y.; Hara, M.; Tojo, S.; Majima, T. *J. Am. Chem. Soc.* **2002**, *124*, 3586−3590.
(39) Kanvah, S.; Schuster, G. B. *J. Am. Chem. Soc.* **2004**, *126*, 7341−7344.
(40) Joseph, J.; Schuster, G. B. *Photochem. Photobiol. Sci.* **2012**, *11*, 998−1003.
(41) Chen, Z. X.; Riggs, A. D. *Biochem. Cell Biol.* **2005**, *83*, 438−448.
(42) Taberlay, P. C.; Jones, P. A. *Prog. Drug Res.* **2011**, *67*, 1−23.
(43) Pfeifer, G. P.; Tang, M.; Denissenko, M. F. *Curr. Top. Microbiol. Immunol.* **2000**, *249*, 1−19.
(44) Chan, W.; Chen, B.; Wang, L.; Taghizadeh, K.; DeMott, M. S.; Dedon, P. C. *J. Am. Chem. Soc.* **2010**, *132*, 6145−6153.
(45) Margolin, Y.; Dedon, P. C. *Methods Mol. Biol.* **2010**, *610*, 325−340.
(46) Krokeide, S. Z.; Laerdahl, J. K.; Salah, M.; Luna, L.; Cederkvist, F. H.; Fleming, A. M.; Burrows, C. J.; Dalhus, B.; Bjoras, M. *DNA Repair (Amsterdam)* **2013**.
(47) Henderson, P. T.; Delaney, J. C.; Gu, F.; Tannenbaum, S. R.; Essigmann, J. M. *Biochemistry* **2002**, *41*, 914−921.
(48) Neeley, W. L.; Essigmann, J. M. *Chem. Res. Toxicol.* **2006**, *19*, 491−505.
(49) Lim, K. S.; Cui, L.; Taghizadeh, K.; Wishnok, J. S.; Chan, W.; DeMott, M. S.; Babu, I. R.; Tannenbaum, S. R.; Dedon, P. C. *J. Am. Chem. Soc.* **2012**, *134*, 18053−18064.
(50) Lim, K. S.; Taghizadeh, K.; Wishnok, J. S.; Babu, I. R.; Shafirovich, V.; Geacintov, N. E.; Dedon, P. C. *Chem. Res. Toxicol.* **2012**, *25*, 366−373.
(51) Tretyakova, N. Sequence distribution of nucleobase adducts studied by isotope labeling of DNA-mass spectrometry.; In *Mass Spectrometry of Nucleosides and Nucleic Acids*; Banoub, J. H., Limbach, P. A., Eds.; CRC Press: Boca Raton, FL, 2009.
(52) Tretyakova, N.; Matter, B.; Jones, R.; Shallop, A. *Biochemistry* **2002**, *41*, 9535−9544.
(53) Tretyakova, N.; Villalta, P. W.; Kotapati, S. *Chem. Rev.* **2013**, *113*, 2395−2436.
(54) Tretyakova, N.; Goggin, M.; Sangaraju, D.; Janis, G. *Chem. Res. Toxicol.* **2012**, *25*, 2007−2035.

(55) Shallop, A. J.; Gaffney, B. L.; Jones, R. A. *J. Org. Chem.* **2003**, *68*, 8657−8661.
(56) Zhao, H.; Pagano, A. R.; Wang, W.; Shallop, A.; Gaffney, B.; Jones, R. A. *J. Org. Chem.* **1997**, *62*, 7832−7835.
(57) Wojciechowski, F.; Hudson, R. H. *Org. Lett.* **2009**, *11*, 4878−4881.
(58) Guza, R.; Kotandeniya, D.; Murphy, K.; Dissanayake, T.; Lin, C.; Giambasu, G. M.; Lad, R. R.; Wojciechowski, F.; Amin, S.; Sturla, S. J.; Hudson, R. H.; York, D. M.; Jankowiak, R.; Jones, R.; Tretyakova, N. Y. *Nucleic Acids Res.* **2011**, *39*, 3988−4006.
(59) Matter, B.; Wang, G.; Jones, R.; Tretyakova, N. *Chem. Res. Toxicol.* **2004**, *17*, 731−741.
(60) Rajesh, M.; Wang, G.; Jones, R.; Tretyakova, N. *Biochemistry* **2005**, *44*, 2197−2207.
(61) Ziegel, R.; Shallop, A.; Jones, R.; Tretyakova, N. *Chem. Res. Toxicol.* **2003**, *16*, 541−550.
(62) Saito, I.; Nakamura, T.; Nakatani, K. *J. Am. Chem. Soc.* **2000**, *122*, 3001−3006.
(63) Naseem, I.; Ahmad, M.; Hadi, S. M. *Biosci. Rep.* **1988**, *8*, 485−492.
(64) Jones, P. A.; Takai, D. *Science* **2001**, *293*, 1068−1070.
(65) Tornaletti, S.; Pfeifer, G. P. *Oncogene* **1995**, *10*, 1493−1499.
(66) Hussain, S. P.; Hollstein, M. H.; Harris, C. C. *Ann. N.Y. Acad. Sci.* **2000**, *919*, 79−85.
(67) Tretyakova, N.; Guza, R.; Matter, B. *Nucleic Acids Symp. Ser. (Oxford)* **2008**, 49−50.
(68) Denissenko, M. F.; Chen, J. X.; Tang, M. S.; Pfeifer, G. P. *Proc. Natl. Acad. Sci. U.S.A.* **1997**, *94*, 3893−3898.
(69) Denissenko, M. F.; Pao, A.; Tang, M.; Pfeifer, G. P. *Science* **1996**, *274*, 430−432.
(70) Hainaut, P.; Pfeifer, G. P. *Carcinogenesis* **2001**, *22*, 367−374.
(71) Hernandez-Boussard, T.; Rodriguez-Tome, P.; Montesano, R.; Hainaut, P. *Hum. Mutat.* **1999**, *14*, 1−8.
(72) Lee, Y. A.; Liu, Z.; Dedon, P. C.; Geacintov, N. E.; Shafirovich, V. *ChemBioChem* **2011**, *12*, 1731−1739.
(73) Gackowski, D.; Speina, E.; Zielinska, M.; Kowalewski, J.; Rozalski, R.; Siomek, A.; Paciorek, T.; Tudek, B.; Olinski, R. *Cancer Res.* **2003**, *63*, 4899−4902.
(74) Loft, S.; Vistisen, K.; Ewertz, M.; Tjonneland, A.; Overvad, K.; Poulsen, H. E. *Carcinogenesis* **1992**, *13*, 2241−2247.
(75) Park, J. H.; Gopishetty, S.; Szewczuk, L. M.; Troxel, A. B.; Harvey, R. G.; Penning, T. M. *Chem. Res. Toxicol.* **2005**, *18*, 1026−1037.
(76) Yu, D. S.; Berlin, J. A.; Penning, T. M.; Field, J. *Chem. Res. Toxicol.* **2002**, *15*, 832−842.
(77) Pryor, W. A.; Prier, D. G.; Church, D. F. *Environ. Health Perspect.* **1983**, *47*, 345−355.
(78) Halliwell, B.; Gutteridge, J. M.; Cross, C. E. *J. Lab. Clin. Med.* **1992**, *119*, 598−620.
(79) Prieme, H.; Loft, S.; Klarlund, M.; Gronbaek, K.; Tonnesen, P.; Poulsen, H. E. *Carcinogenesis* **1998**, *19*, 347−351.
(80) Xie, Y.; Yang, H.; Cunanan, C.; Okamoto, K.; Shibata, D.; Pan, J.; Barnes, D. E.; Lindahl, T.; McIlhatton, M.; Fishel, R.; Miller, J. H. *Cancer Res.* **2004**, *64*, 3096−3102.
(81) Harris, C. C. *J. Natl. Cancer Inst.* **1996**, *88*, 1442−1455.
(82) Fritsche, M.; Haessler, C.; Brandner, G. *Oncogene* **1993**, *8*, 307−318.
(83) Pfeifer, G. P.; Denissenko, M. F.; Olivier, M.; Tretyakova, N.; Hecht, S. S.; Hainaut, P. *Oncogene* **2002**, *21*, 7435−7451.
(84) Hussain, S. P.; Harris, C. C. *Mutat. Res., Fundam. Mol. Mech. Mutagen.* **1999**, *428*, 23−32.
(85) Greenblatt, M. S.; Bennett, W. P.; Hollstein, M.; Harris, C. C. *Cancer Res.* **1994**, *54*, 4855−4878.
(86) Yu, H.; Venkatarangan, L.; Wishnok, J. S.; Tannenbaum, S. R. *Chem. Res. Toxicol.* **2005**, *18*, 1849−1857.
(87) Fleming, A. M.; Muller, J. G.; Dlouhy, A. C.; Burrows, C. J. *J. Am. Chem. Soc.* **2012**, *134*, 15091−15102.
(88) Schuster, G. B. *Nucleic Acids Symp. Ser. (Oxford)* **2009**, 85−86.
(89) Odom, D. T.; Barton, J. K. *Biochemistry* **2001**, *40*, 8727−8737.
(90) Valinluck, V.; Tsai, H. H.; Rogstad, D. K.; Burdzy, A.; Bird, A.; Sowers, L. C. *Nucleic Acids Res.* **2004**, *32*, 4100−4108.
(91) Dannenberg, J. J.; Tomasz, M. *J. Am. Chem. Soc.* **2000**, *122*, 2062−2068.
(92) Hausheer, F. H.; Rao, S. N.; Gamcsik, M. P.; Kollman, P. A.; Colvin, O. M.; Saxe, J. D.; Nelkin, B. D.; McLennan, I. J.; Barnett, G.; Baylin, S. B. *Carcinogenesis* **1989**, *10*, 1131−1137.
(93) Norberg, J.; Vihinen, M. *J. Mol. Struct.: THEOCHEM* **2001**, *546*, 51−62.
(94) Manthey, K. C.; Chew, Y. C.; Zempleni, J. *J. Nutr.* **2005**, *135*, 978−982.
(95) Liu, G.; Lu, C.; Yao, S.; Zhao, F.; Li, Y.; Meng, X.; Gao, J.; Cai, J.; Zhang, L.; Chen, Z. *Sci. China, Ser. C: Life Sci.* **2002**, *45*, 344−352.
(96) Guza, R.; Ma, L.; Fang, Q.; Pegg, A. E.; Tretyakova, N. *J. Biol. Chem.* **2009**, *284*, 22601−22610.